Journal of Nuclear Science and Technology

ISSN: 0022-3131 (Print) 1881-1248 (Online) Journal homepage: https://www.tandfonline.com/loi/tnst20

Numerical analysis of RBHT reflood experiments using MARS 1D and 3D modules

Gwang Hyeok Seo, Hong Hyun Son & Sung Joong Kim

To cite this article: Gwang Hyeok Seo, Hong Hyun Son & Sung Joong Kim (2015) Numerical analysis of RBHT reflood experiments using MARS 1D and 3D modules, Journal of Nuclear Science and Technology, 52:1, 70-84, DOI: 10.1080/00223131.2014.932722

To link to this article: https://doi.org/10.1080/00223131.2014.932722

Journal of Nuclear Science and Technology, 2015
Vol. 52, No. 1, 70–84, http://dx.doi.org/10.1080/00223131.2014.932722

Taylor & Francis
Taylor & Francis Group

ARTICLE

Numerical analysis of RBHT reflood experiments using MARS 1D and 3D modules

Gwang Hyeok Seo, Hong Hyun Son and Sung Joong Kim*

Department of Nuclear Engineering, Hanyang University, 222 Wangsimni-ro, Seongdong-gu, Seoul 133-791, Republic of Korea

(*Received 17 December 2013; accepted final version for publication 28 May 2014*)

The Rod Bundle Heat Transfer (RBHT) program was performed experimentally to analyze the reflood heat transfer phenomena under the conditions of reflood phase following a hypothesized loss of coolant accident (LOCA) by the team of Penn State University. In order to verify the experimental data using a numerical analysis, the Multi-dimensional Analysis of Reactor Safety (MARS) assessment of the RBHT experimental data was carried out for the flooding rates of 0.0254 and 0.1524 m/sec with the upper plenum pressure of 276 kPa. The RBHT experimental data of Tests 1285 and 1383 were compared with the calculation results of the MARS 1D and 3D modules. The MARS code shows a good agreement in the general trend of the peak cladding temperatures although there are limitations in predicting accurate quenching time for both modules. However, in comparison to the MARS 1D module simulation, the MARS 3D module shows the improved calculation capability in that the code can capture local enhanced heat transfer with implication of spacer grids. Moreover, the temperature profiles simulated by the 3D module show the accurate prediction at which the local peak temperatures occur. For more enhanced simulations, local flow parameters such as cross flow and vortex flow need to be analyzed for a more accurate prediction of quenching behavior.

Keywords: thermal-hydraulics; rod bundle; numerical simulation; quench; entrainment; LOCA

1. Introduction

Reflood phenomenon is the heat transfer mode describing cold water injection over the overheated structures or fuel assemblies of the nuclear reactor. It involves complicated heat transfer phenomena of two-phase mixtures in terms of liquid–vapor phase change and corresponding mass, momentum, and energy transfer within the confined geometry of the flow channels. The reflood phase may occur during hypothesized design basis accidents (DBAs) such as loss of coolant accident (LOCA) and loss of flow accident (LOFA) as a result of proper safety flow injection. Thus, it is considered one of the most important thermal-hydraulic (T/H) phenomena requiring physical understanding due to its significance and complexity.

In an effort to understand the complex heat transfer in the reflood phase, many research works have been carried out using various experimental facilities. An experimental investigation on the reflood phase with a rod bundle was conducted through the Full-Length Emergency Cooling Heat-Transfer-Separate-Effects and Systems-Effects Test (FLECHT-SEASET) programs in the 1970s. Overall, reflood heat transfer mechanism within the core was examined using the data obtained from the FLECHT-SEASET tests [1]. However, it was insufficient to quantify the phenomena relevant to detailed reflood mechanism due to some uncertainties generated in the experiment, which hinders the development and validation of more reliable reflood model [1]. The FEBA reflood experiments were carried out to investigate the effectiveness of the emergency core cooling of pressurized water reactors (PWRs) at KfK, Germany in 1977. The objective of the test program was to study heat transfer mechanism for the development and assessment of improved T/H models [2]. Moreover, the test series performed with the 5 × 5 rod bundle and spacer grids were conducted to examine the grid effect during the reflood phase [3]. In the 1980s, the PERICLES reflood experiments were performed at CEA Grenoble, France, aiming at studying multi-dimensional effects, which include cross flows of water and steam, and fallback of water from the upper plenum to the core. The experimental data have been used to develop suitable reflood models for system safety analysis codes [4]. In spite of various activities related to the verification of reflood heat transfer, however, it is still

*Corresponding author. Email: sungjkim@hanyang.ac.kr

questionable if solid understanding of the phenomenon is established well with incorporation of complex heat transfer mechanisms. To better understand the reflood phenomena, the Rod Bundle Heat Transfer (RBHT) facility was designed by the team of Penn State University with a special focus on development and validation of the reflood model [5]. It is delicately instrumented to collect a large set of reliable data related to the local thermal-hydraulic phenomena of the reflood heat transfer.

The obtained experimental database provides valuable information on developing and validating current reflood models implemented in several nuclear system safety codes. Most of the standard system safety codes, such as RELAP5 (USA) and CATHARE (France) series, adopted two field models for two-phase flow calculations. With enormous assessment works, the system safety codes have been modified and improved to date. For example, Choi and No modified and assessed the reflood model implemented in RELAP5/MOD3.3 using the FLECHT-SEASET and RBHT experimental data [6,7]. To improve quenching behavior predicted by the code, the film boiling heat transfer regime was divided into three separate regimes depending on void fraction, and an assessment work for eight FLECHT-SEASET tests was conducted. Their study showed an improved prediction of peak cladding temperatures (PCTs) and quenching times although earlier quenching behavior was still the unsolved problem with the modified code [6]. In addition, nuclear system safety codes adopting a three-field model, such as COBRA-TF (USA), CATHARE3 (France), and SPACE (Korea), have been under development for accurate simulation of thermal-hydraulic phenomena. Since the three-field model deals with a separate droplet field with gas and continuous liquid fields, it has a substantial advantage when a large amount of droplets works as the dominant heat transfer medium. During the blowdown and reflood phases, many droplets are expected to appear in the region of dispersed flow film boiling (DFFB), which occurs at the high local void fraction greater than 80% and a rod wall temperature above minimum film boiling temperature [3,8–11]. In this flow regime, poor heat transfer leads to the PCT. On the contrary, when the wall temperature decreases below minimum film boiling temperature, a sudden decrease of a rod cladding temperature at the quench front is observed [3]. **Figure 1** shows the aforementioned flow regimes for the bottom reflood case. Of importance is that the nuclear system safety codes having the three-field model may contribute on simulating more realistic thermal-hydraulic phenomena including accurate predictions of PCT and quenching behavior. Thus, the DFFB model in the COBRA-TF code has been improved using the RBHT experimental data. Ergun et al. introduced a new small droplet field, modifying the other three fields (vapor, liquid, and large droplet) in their recent assessment work on a modification of COBRA-TF [9–11]. Adding the small droplet field led to improved predictions of the quenching time and droplet entrainment at the quench front. However, the earlier quenching is still observed in the original and modified versions of the code. They concluded that the new droplet field worked reasonably well and minimum film boiling temperature model needed to be improved.

In Korea, the Multi-dimensional Analysis of Reactor Safety (MARS) code has been widely used as the best estimate code for system safety analysis, and the reflood model implemented in the same code has not been validated sufficiently enough for accurate prediction of the reflood phenomena. Furthermore, since the MARS code was developed from the RELAP5/MOD3 code for one-dimensional (1D) thermal-hydraulic module and the COBRA-TF code for three-dimensional (3D) thermal-hydraulic module [12–15], reported limitations observed from the previous studies with other safety codes are expected to exist in the MARS code. Therefore, the objective of this study is to validate the MARS code predictability to quenching behavior using the RBHT experimental data and to clarify influences of the code's grid model to local thermal-hydraulic phenomena. In order to improve the prediction capability, the hot channel analysis module of the MARS code, i.e., the MARS 3D module has been adopted in comparison with the MARS 1D module. Two representative tests were selected from the RBHT experiments. Test 1383 for lower flooding rate (0.0254 m/sec) and Test 1285 for higher flooding rate (0.1524 m/sec) are validated through the MARS 1D and 3D modules. Ergun et al.'s study validated only low flow conditions (Test 1383) and this study is to cover both low and high flow conditions because the thermal-hydraulic assessment of the safety code often characteristically differs with the flow regimes. Comparison of the results by the 1D and 3D modules and the experimental data is expected to provide critical judgment on prediction capability of the MARS code.

2. Description of RBHT reflood experiment

The RBHT facility consists of a test section, coolant injection and steam injection systems, steam separator, and steam collection tanks [16–18]. In essence, the test section was designed and fabricated for the purpose of visual observation for various reflood experiments. A schematic view of the test facility is presented in **Figure 2** and an isometric view of the test section is given in **Figure 3**. The test section includes the heater rod bundles, flow housing, and lower and upper plena. Forty-five heater rods and four unheated supporting rods are arranged in a 7×7 bundle array, which simulates a part of a 17×17 PWR fuel assembly. The heater rods have a diameter of 9.50 mm (0.374 in) and 3.66 m (144 in) of heated length. The heater rod consists of four segments: boron nitride (BN) insulation, Monel K-500 resistance element, BN insulation, and Inconel 600 cladding from the inner part. The supporting rods of diameter 9.30 mm (0.366 in) are used to support the rod bundle and fluid thermocouple leads.

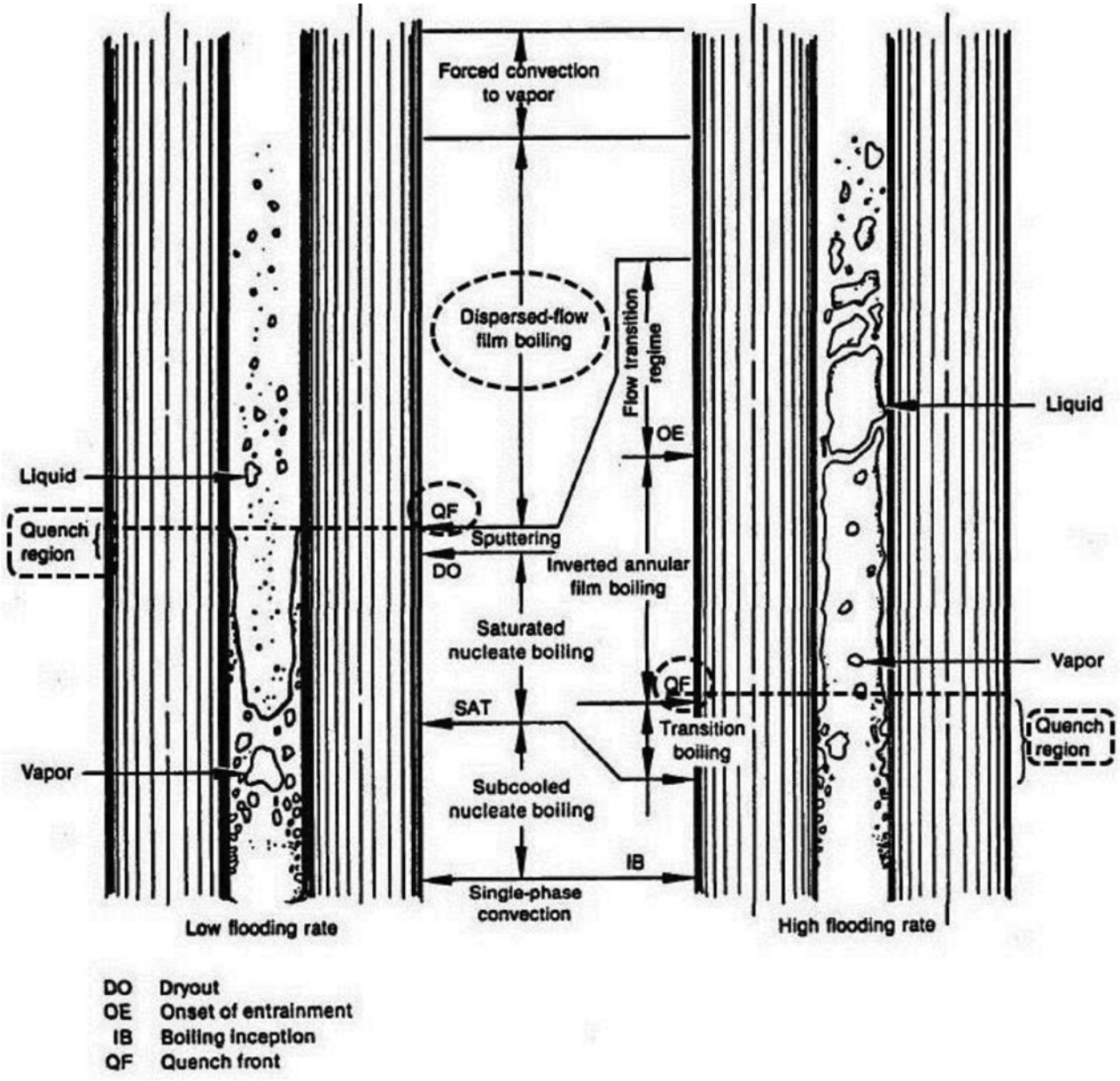

Figure 1. Heat transfer and hydraulic flow regimes for bottom reflood [3].

Each heater rod is electrically heated up and a uniform radial power distribution is maintained effectively during a test. However, as seen in **Figure 4**, the axial power distribution exhibits a shape skewed to the bottom with a sharp peak at 2/3 of the total heated length. The maximum to average power ratio (P_{max}/P_{avg}) is 1.5 at 2.74 m (108 in) and the minimum to average power ratio (P_{min}/P_{avg}) is 0.5 at both ends of the heated length. Furthermore, seven mixing vane grids similar to those used in the typical 17 × 17 PWR fuel assembly are placed at various elevations of the rod bundle. The elevations of the grids are shown in **Table 1**. The flow housing was designed for providing pressure and flow boundary for the rod bundle. It is made of Inconel 600, which is the same material of the heater rod cladding. The flow housing has a square shape with inside dimension of 90.17 × 90.17 mm^2 (3.550 × 3.550 in^2).

Total 512 data channels are instrumented for the RBHT facility to obtain various experimental data of temperatures, pressures, and flow rates, to mention a few. Forty-nine rods of the rod bundle part are grouped in accordance with their role: eight heater rod groups numbered 1–8, one unheated rod group marked as 'X' and one un-instrumented rod group marked as '0' as shown in **Figure 5**.

The thermocouples of each group are installed to measure wall temperatures of the rods. They are concentrated on specific axial positions of the heater except those of group 7. Eight thermocouples are assigned to each heater rod group (1–8). Thus total 248 thermocouples are attached to the 31 heater rods. In addition, the unheated rod group or the support rod group (X) includes 16 thermocouples, and no thermocouple is attached to the un-instrumented rod group (0). The axial

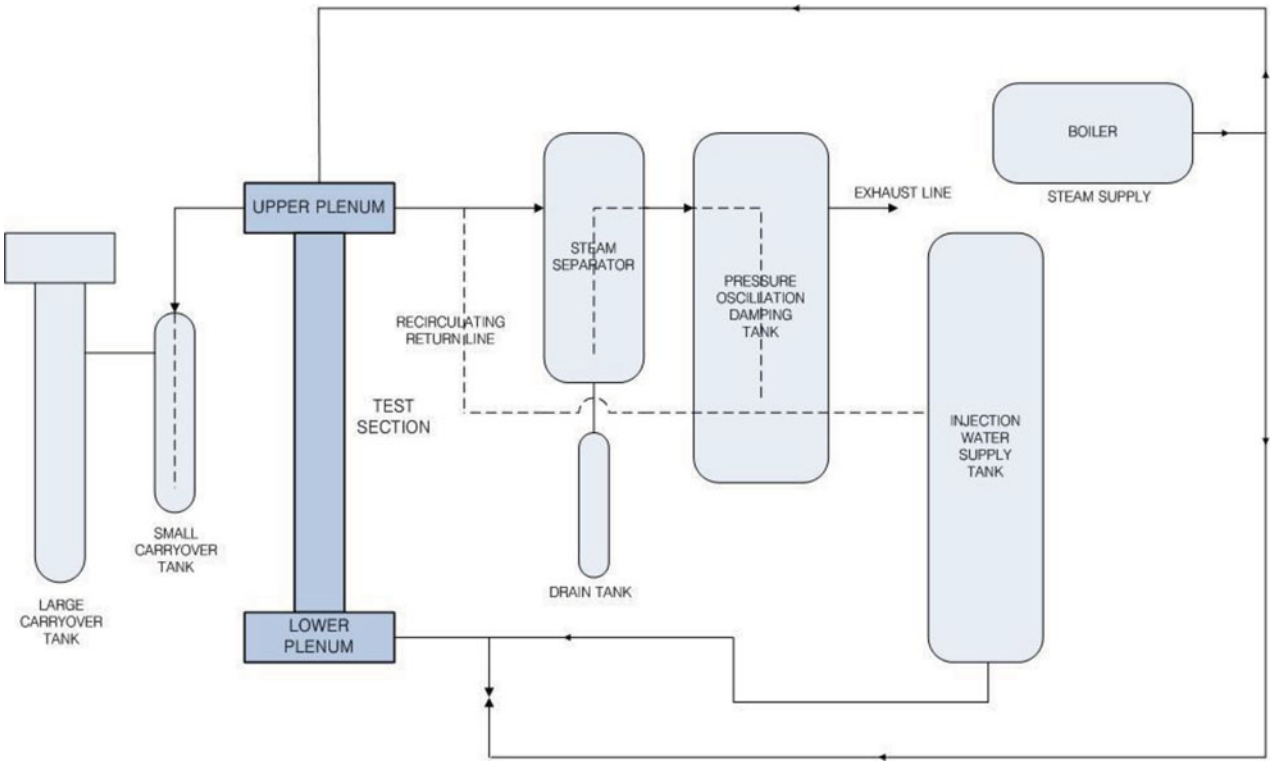

Figure 2. Schematic view of the RBHT facility [16–18].

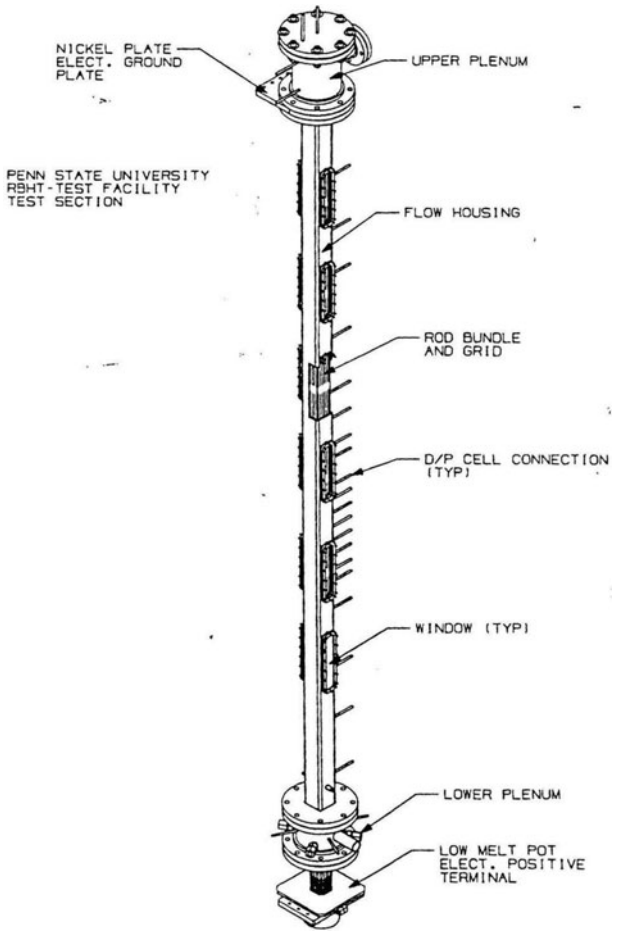

Figure 3. Isometric view of the test section [16–18].

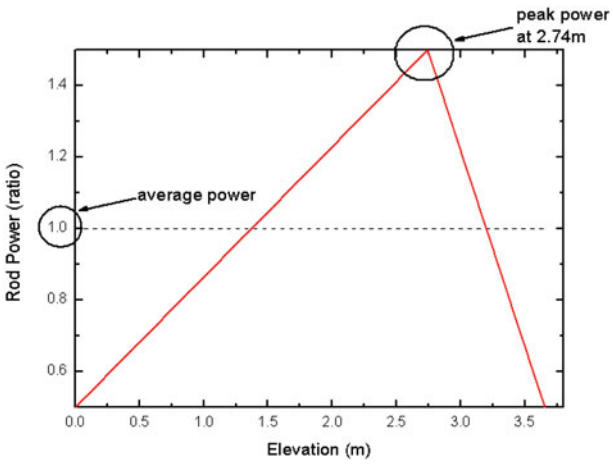

Figure 4. Axial power distribution [16–18].

locations of all the thermocouples are shown in **Figure 6**. The volume number represents the axial nodes in the modeling of the MARS 1D module. The flow housing has 25 thermocouples at various elevations for measuring the housing wall temperatures.

3. MARS code structure and models

3.1. Overview of MARS code structure

The MARS code consists of two thermal-hydraulic analysis codes, which are the RELAP5/MOD3 code for

Table 1. Elevations of seven spacer grids.

Grid no.	Elevation (m)
Grid 1	0.10–0.14
Grid 2	0.65–0.69
Grid 3	1.14–1.18
Grid 4	1.75–1.79
Grid 5	2.20–2.24
Grid 6	2.81–2.85
Grid 7	3.34–3.38

1D thermal-hydraulic module and the COBRA-TF code for 3D thermal-hydraulic module [12–15]. Since the two codes were consolidated into a single code, MARS provides the calculation capability of not only coolant system analysis but also hot channel analysis. The MARS 3D module uses a three-field (gas, liquid, and droplets) model for the two-phase flow calculations on rectangular Cartesian or subchannel coordinates. In the modeling process, input decks for the MARS 1D and 3D modules were prepared separately in order to model the test section of the RBHT facility.

3.2. *Brief description of MARS hydrodynamic models for DFFB*

In the assessment studies, Ergun et al. suggested that key models affecting DFFB were the following models: minimum film boiling temperature, entrainment, and droplet interfacial drag coefficient models. When wall temperature of a rod decreases below the minimum film boiling temperature, heat transfer mode changes from film boiling to transition boiling as shown in Figure 1. As a result, the wall temperature decreases quickly. Thus, the minimum film boiling temperature affects the quench front behavior [3].

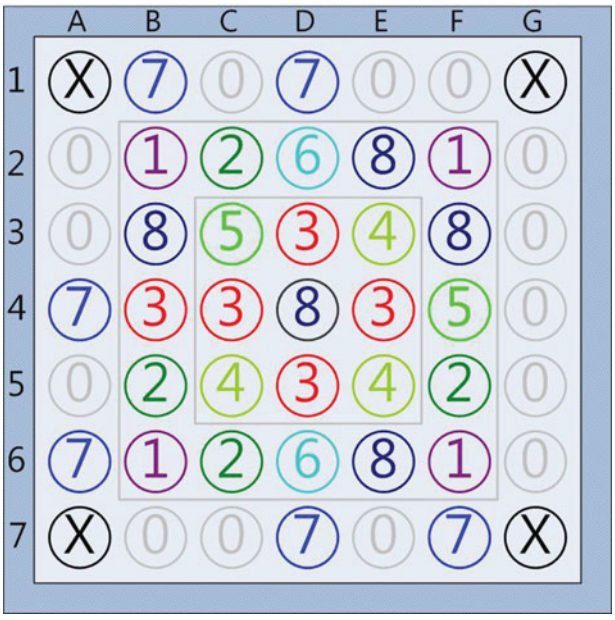

Figure 5. Rod bundle arrangement and rod group [16–18].

Moreover, vapor generated at the quench front as shown in Figure 1 entrains water fragments and droplets. The droplets entrained by the vapor as well as the water fragments in the DFFB regime participate in considerable amounts of heat transfer for local cooling [3]. In the MARS 3D module, droplet entrainment by vapor bubbling through liquid pool is considered for bottom reflood. The entrainment rate (S_E) is given by

$$S_E = \left(\frac{\alpha_v u_v}{u_{\text{crit}}}\right)^2 \dot{m}_v \tag{1}$$

$$u_{\text{crit}} = \left(\frac{4\text{We}_d}{3C_D}\right)^{1/4} \left(\frac{\sigma g \Delta\rho}{\rho_v^2}\right)^{1/4} \tag{2}$$

where $\dot{m}_v$ is the vertical vapor mass flow rate, and u_{crit} is the critical velocity, which is the vertical vapor velocity required to drag a droplet with radius defined by the critical Weber criterion against gravity. A Weber number (We_d) of 2.7 is used, which is a typical value of reflood in the FLECHT tests [13]. As Equations (1) and (2) indicate, the entrainment is mainly affected by the critical velocity, u_{crit}, and the quenching behavior for a hot rod varies with a prediction of u_{crit}. For example, the underestimated u_{crit} increases the entrainment rate, which, in turn, causes the PCT to decrease. However, a rise of the quench front upward is delayed. As a result, the quenching time is observed to be slower, and vice versa [19].

In addition, since vapor moves upward with dragging droplets, interfacial drag between the vapor and droplets affects the time in which the droplets remain in a rod bundle [8,9]. The droplet interfacial drag coefficient in the MARS 3D module is given by

$$C_D = \max\left[0.45, \frac{24}{\text{Re}_D}\left(1 + 0.1\text{Re}_D^{0.75}\right)\right] \tag{3}$$

where Re_D is the Reynolds number of the droplet field [13]. As shown in the analysis of Ergun et al., once the interfacial drag is overpredicted, the droplets dragged by vapor move out of the bundle quickly, and the amount of droplets is underpredicted. As a result, the delayed quenching time is predicted, and vice versa [9,10,13].

4. Numerical modeling for the RBHT experiments

4.1. *Input model for the MARS 1D module*

For the MARS simulation, the test section of the RBHT facility is modeled as three hydrodynamic components and three heat structures. A schematic view of the test section modeling is shown in **Figure 7**. Also, the nodalization for the MARS 1D module is presented in Figure 7. The rod bundle part is modeled as a pipe component having 20 volumes and 19 junctions. A time-dependent volume and a time-dependent junction are

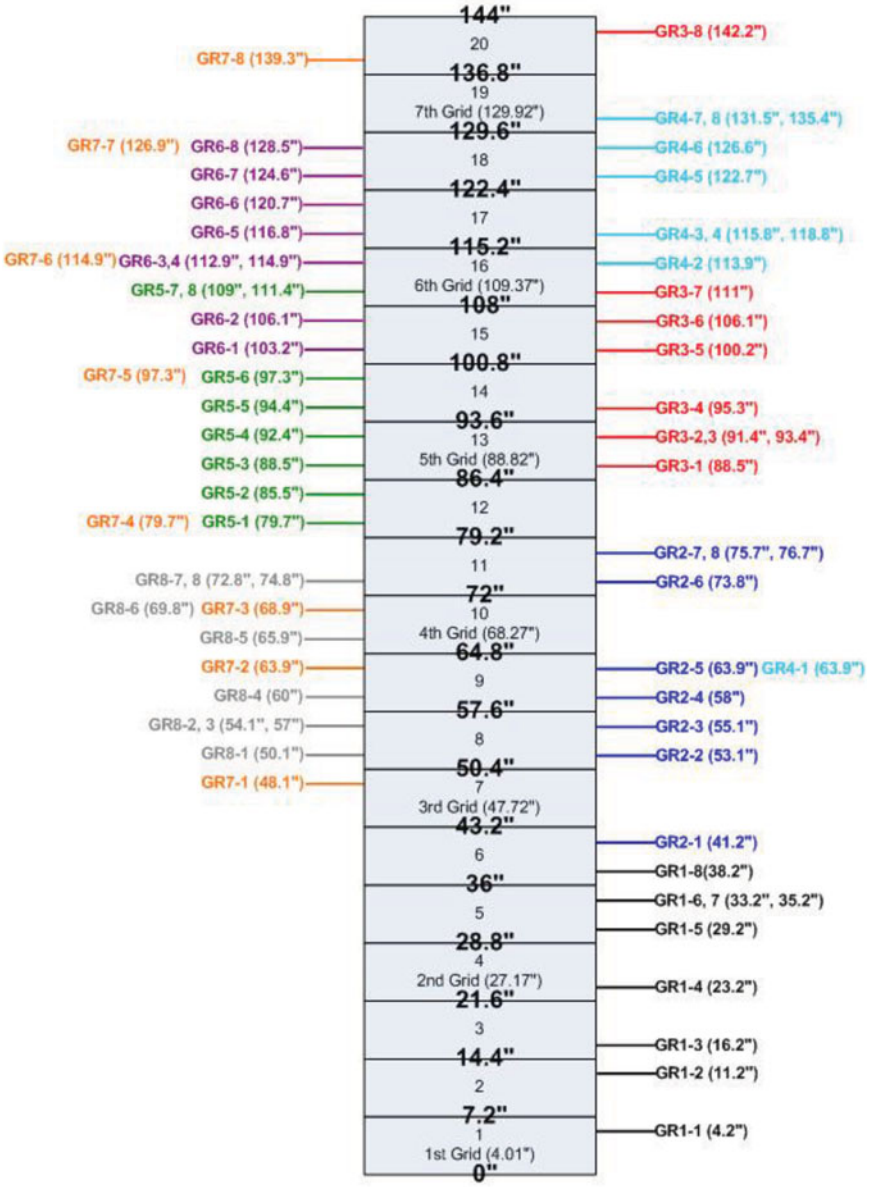

Figure 6. Axial locations of the thermocouples corresponding to MARS 1D nodalization.

assigned to the lower plenum. The upper plenum is represented by a time-dependent volume and a single junction. A flow rate is defined at the time-dependent junction in the lower plenum part. Pressure boundary condition is applied to the upper plenum part. The applied initial and boundary conditions are the same as the experimental conditions represented in **Table 2**. In addition, the seven grid structures are not modeled in this process since there is no grid model in the current MARS 1D module.

The heat structures in the test section are simply classified into 45 heated rods, 4 unheated rods, and the housing wall. Each part is modeled as individual heat structure. Each heat structure is constructed as a total length of 3.66 m (144 in), which are divided in 20 axial nodes. Each axial node has an equal length of 0.18 m (7.2 in).

The radial nodal view of the heater rods having eight nodes is shown in **Figure 8**. For the first two parts of BN and Monel K-500, one equal node was allocated. For the latter two parts (BN and Inconel 600) three equal nodes were assigned. The modeling of the unheated rods is the same as that of the heater rods except that three radial nodes are assigned to them equally.

The modeling of the flow housing is presented in **Figure 9**. The housing wall shaded in Figure 9(a) is modeled as a square pillar considering the housing area and the wetted part with coolant. It consists of 20 equal axial nodes and three radial nodes. Each volume has a length of 0.18 m (7.2 in) because the housing wall is modeled to have a length of 3.66 m (144 in), which is the same as that of the rod bundle part.

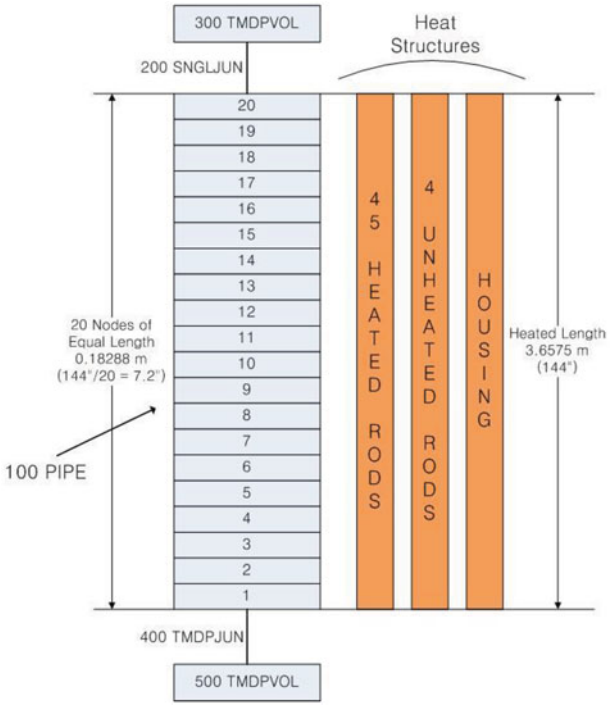

Figure 7. Nodalization for the MARS 1D module.

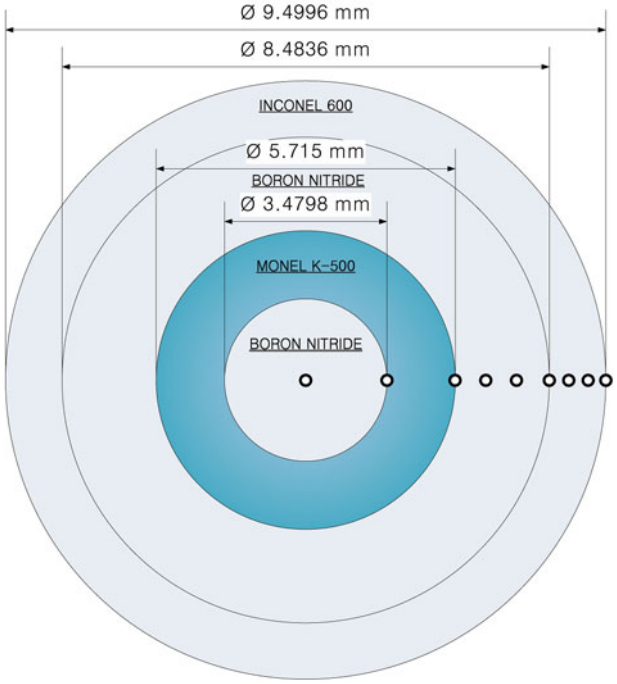

Figure 8. Radial nodal scheme of the heater rods.

4.2. *Input model for the MRAS 3D module*

In order to confirm the calculation capability of subchannel analysis, the test section is also modeled using the MARS 3D module. In general, the input model of the MARS 3D module is similar to that of the MARS 1D module in terms of the test section dimensions and experimental conditions. The applied initial and boundary conditions are also the same as the experimental conditions described in Table 2. However, significant efforts

Table 2. Experimental conditions for RBHT Tests 1285 and 1383.

	Test 1285	Test 1383
Upper plenum pressure (kPa)	276	276
Initial peak clad temperature (K)	1144	1033
Rod peak power (kW/m)	2.3	1.31
Flooding rate (m/sec)	0.1524	0.0254
Inlet subcooling (K)	11	11

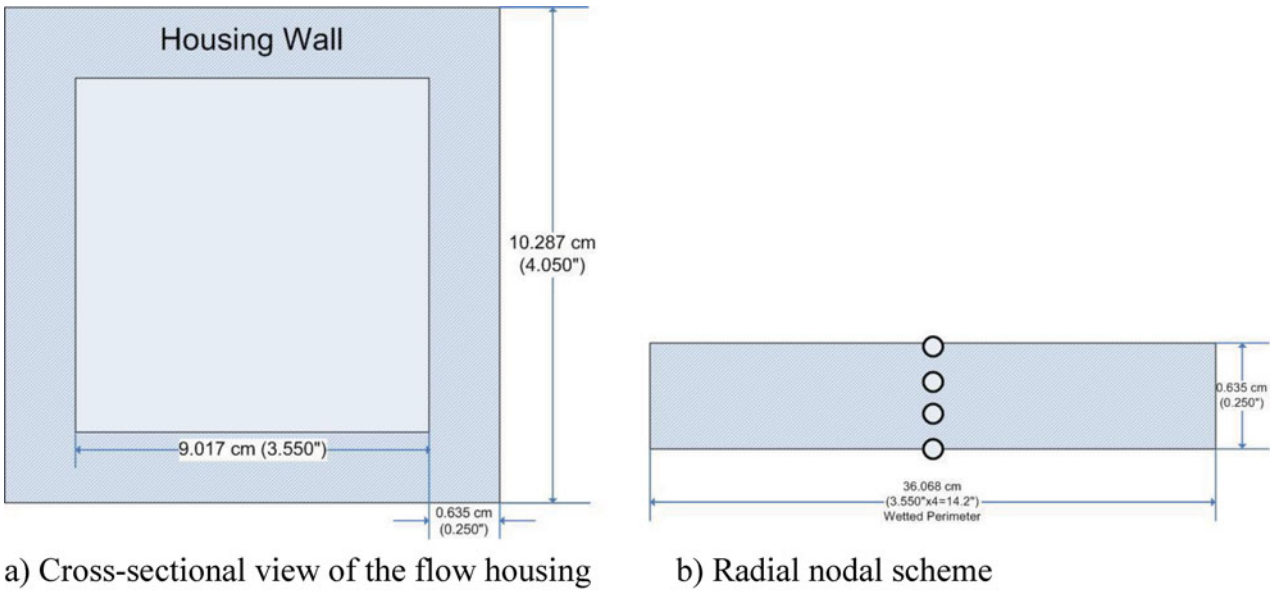

Figure 9. Flow housing nodalization.

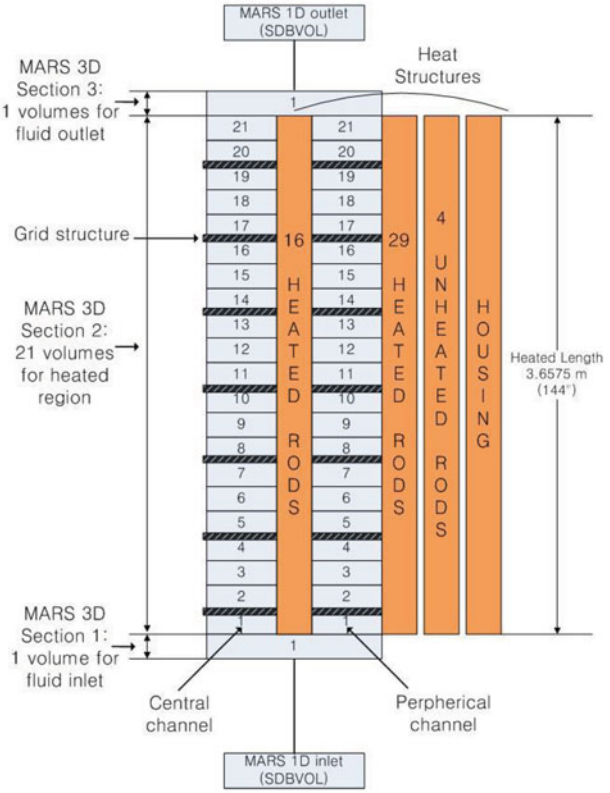

Figure 10. Input model nodalization for the MARS 3D module.

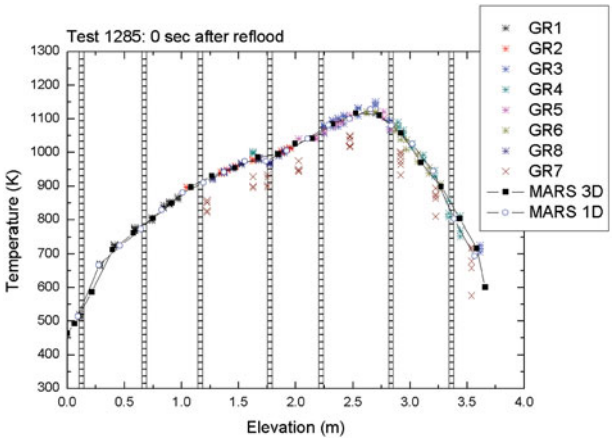

Figure 11. Cladding temperatures with elevation of Test 1285 at 0 sec after reflood.

have been made in constructing the 3D input to properly reflect the 3D effect occurring in the test section. Especially, inclusion of grid model is beneficial in achieving the enhanced prediction results.

In the 3D module modeling, the test section consists of three axial sections and four fluid channels as shown in **Figure 10**. The bottom (section 1) and top (section 3) sections include one fluid channel (channel 1 and 4, respectively), and the center heated section (section 2) is divided into two fluid channels, which are the central (or inner channel: channel 2) and peripheral (or outer channel: channel 3). The central part includes 16 heater rods while the peripheral part encompasses 29 heater rods, four unheated rods and the flow housing. Since the hydrodynamic volumes of the 3D module are connected to the 1D inlet and outlet volumes, two SDBVOL components are used. The lower and upper plena are modeled as 1D PIPE components. Modeling of the heat structures in the 3D module is similar to those of the 1D module. The heater rods are divided into four regions radially, and modeled as the 'hrod' geometry type, which indicates a solid cylinder. The radial nodal view of the heater rods is shown in Figure 8, which is the same as the 1D modeling. The materials of each region are BN, Monel K-500, BN, and Inconel 600 from the innermost. The unheated rods include only the Inconel 600 region and are modeled as the 'tube' geometry type. The flow housing is modeled as the 'wall' geometry type.

Differing from the 1D modeling, seven grids were modeled in the test section for 3D modeling. The grid structure in this 3D modeling is known for enhancing convective heat transfer, which is expected as the additional heat transfer mode during the reflood phase. The grids are located at the interface between nodes of both inner and outer channels. Except for the first grid, three equal nodes are allocated between each grid. Figure 10 shows the positions of the grids, and the elevation and length of the grids are presented in Table 1. The overall modeling is referenced from previous studies and modified for the MARS 3D module [15,20,21].

5. Results and discussion

In order to confirm the calculation capability of the MARS 1D and 3D modules, respectively, simulation results of the code are compared with the experimental data of RBHT Tests 1285 and 1383. The RBHT test conditions are described in Table 2.

The RBHT experiments were conducted using the following procedures. First, heaters are turned on to supply sufficient heat to the test section. After the start of heating, a water coolant is injected from the lower plenum to the bottom of the rod bundle part. Subsequently, the heater rods in the rod bundle part experience rapid quenching and then the coolant injection is terminated.

Figures 11 and 12 show the cladding temperature distribution of the heated rods for Test 1285 (higher flooding rate) and Test 1383 (lower flooding rate), respectively, at the moment of the injection start, which can be expressed as the start of reflood phase. In the figures, symbols '∗' and 'x' represent the experimental data, and symbols '■' and '○' show the simulation results of the 3D and 1D modules, respectively. It is remarked that the heater rods of group 7 (GR7, symbol 'x') have lower cladding temperatures. Since the GR7 rods are positioned in the outer sides of the test section as shown in Figure 5, the heat loss effect occurs during the tests. The

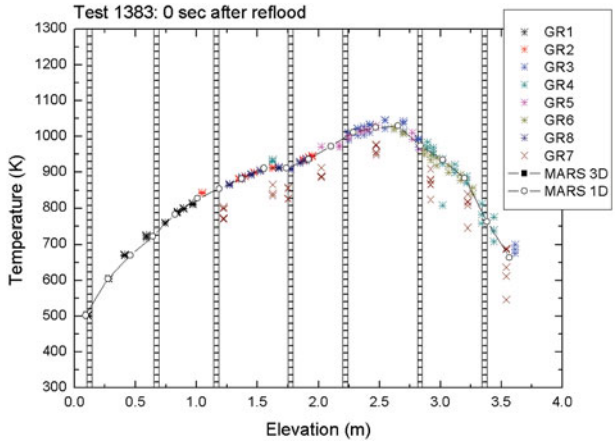

Figure 12. Cladding temperatures with elevation of Test 1383 at 0 sec after reflood.

positions of the seven grids are depicted as the vertical bars. As shown, the temperatures calculated by the 1D and 3D modules along the entire elevation show a good agreement with the experimental data.

5.1. *Comparison results for the higher flooding rate*

Figures 13 and 14 show the cladding temperatures predicted and measured for Test 1285 with time at elevations of 1.35 and 2.69 m, respectively. Elevations of 1.35 and 2.69 m correspond to the axial locations of the average and peak power, respectively, as shown in Figure 4. The calculation results show a good agreement until reaching the maximum temperature or PCT, and then the code predicts earlier quenching of the heater rods than the experiment shows. **Figure 15** shows the entire quench front location calculated by the MARS code with the experimental data [18]. In lower and middle regions of the test section, reasonable quenching times were calculated although slightly fast quenching times

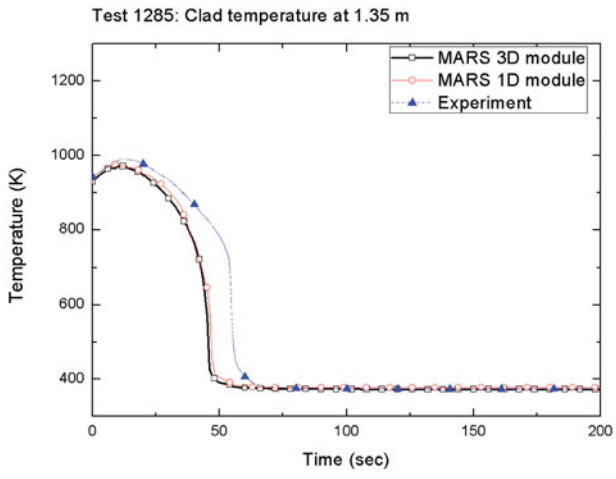

Figure 13. Cladding temperatures with time of Test 1285 at 1.35 m.

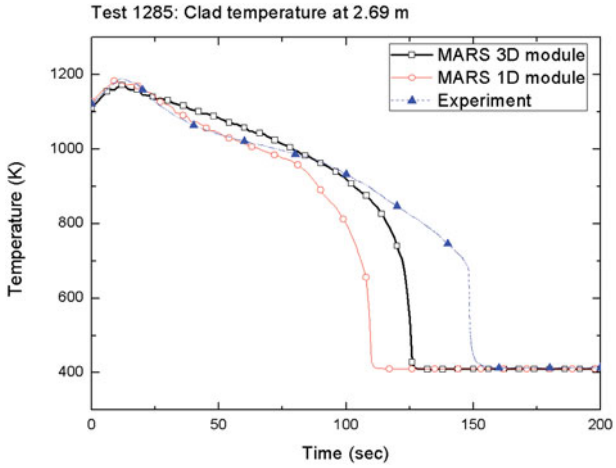

Figure 14. Cladding temperatures with time of Test 1285 at 2.69 m.

were observed for most regions. This faster quenching predicted by both the modules indicates that the minimum film boiling temperature of the heater rods is overpredicted. As mentioned earlier, a rapid decrease of rod wall temperature occurs below the minimum film boiling temperature. Hence, the overestimated minimum film boiling temperatures by the 1D and 3D modules result in the earlier quenching time.

In addition, **Figure 16** shows the vapor temperatures predicted and measured for Test 1285 with time at the elevation of 2.54 m. The code predicts a good agreement until the heater rods reach the PCTs. Since then, a disagreement between the vapor temperatures calculated and the experimental data is observed. The calculation results show a slow and gradual decrease while the experiment shows substantial decrease in the vapor temperatures near 20 sec, which is the moment when the injection flow rate reaches initially the referenced value of 0.74 kg/sec (0.1524 m/sec) after the reflood starts as shown in **Figure 17**. The void fractions calculated by the

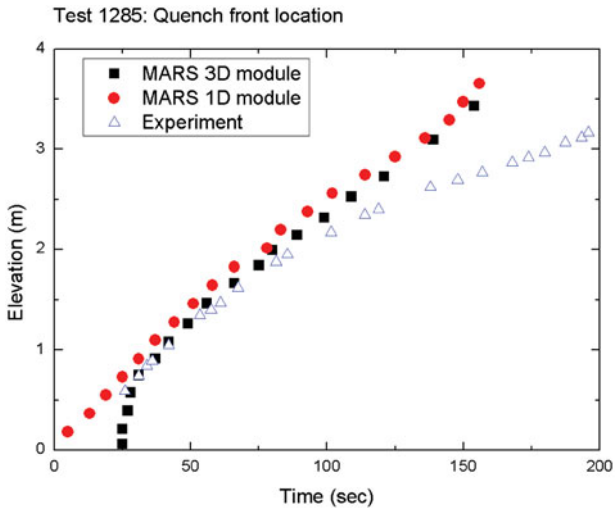

Figure 15. Quench front location of Test 1285.

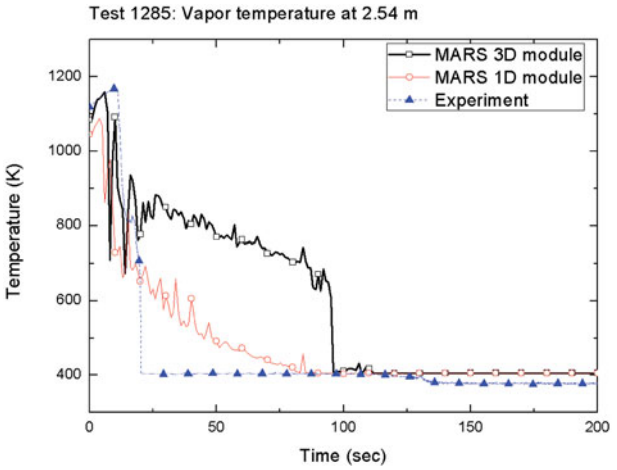

Figure 16. Vapor temperatures with time of Test 1285 at 2.54 m.

MARS code also reflect the tendency of the vapor temperature changes as shown in **Figure 18**. Since more liquid could give active local heat transfer, the void fraction affects cooling pattern of vapor and cladding temperatures. Furthermore, it could be evaluated that predicting the minimum film boiling temperature greatly affects the cooling pattern of the heater rods than that by wall-to-vapor heat transfer since the disagreement in the vapor temperatures does not reflect the tendency of the earlier quenching. Thus, the simulation results indicate that it is needed to improve the minimum film boiling temperature model for the MARS code.

Moreover, Choi and No [6] observed a similar cooling tendency of vapor temperature in a recent assessment work on a modification of the RELAP5/MOD3.3 code using the FLECHT-SEASET experimental data. In their study, the prediction of vapor temperatures by the original and modified versions of the code showed a slow and gradual decrease while a rapid decrease in vapor temperature after reaching the maximum values was observed in the experimental data of Test 31701 [6]. The

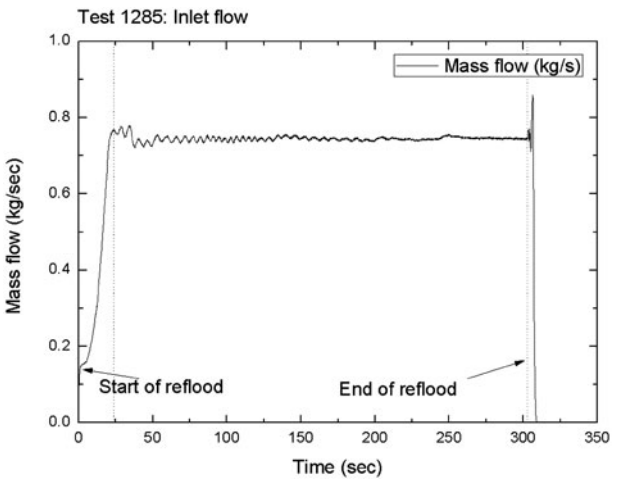

Figure 17. Inlet flow rate with time of Test 1285.

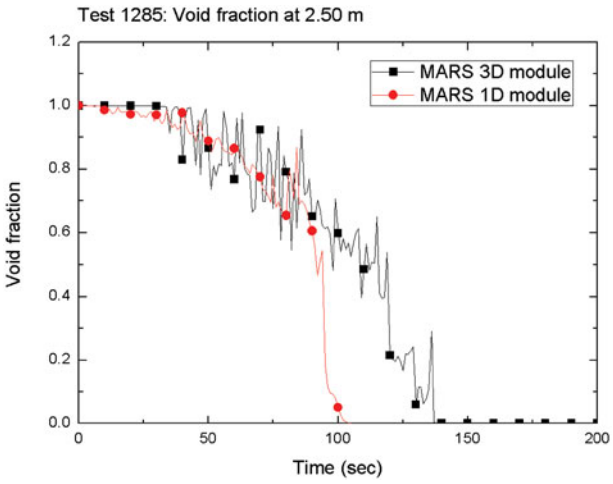

Figure 18. Local void fraction with time of Test 1285 at 2.50 m.

test condition of Test 31701 of the FLECHT-SEASET experiments is the flooding rate of 0.155 m/sec with the upper plenum pressure of 280 kPa, which is also similar to that of Test 1285 of the RBHT experiments.

5.2. *Comparison results for the lower flooding rate*

Figures 19 and 20 show the cladding temperatures predicted and measured for Test 1383 at elevations of 1.35 and 2.69 m, respectively. As similar to the case of Test 1285, the MARS 1D and 3D modules show the similar PCTs to the experimental data although the PCT calculated by the 3D module at 2.69 m is higher than the results by the 1D module and the experiment. Furthermore, like the case of Test 1285, the earlier quenching in the 1D and 3D simulations is observed as well. The simulation results by both the modules show a fast decrease in the cladding temperatures after reaching the PCTs while the experiment shows a different cooling pattern,

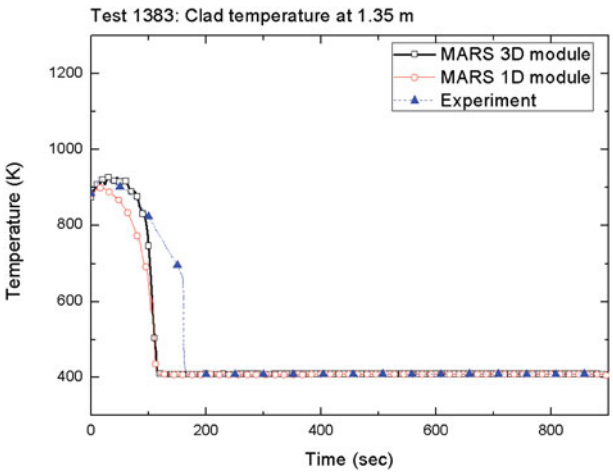

Figure 19. Cladding temperatures with time of Test 1383 at 1.35 m.

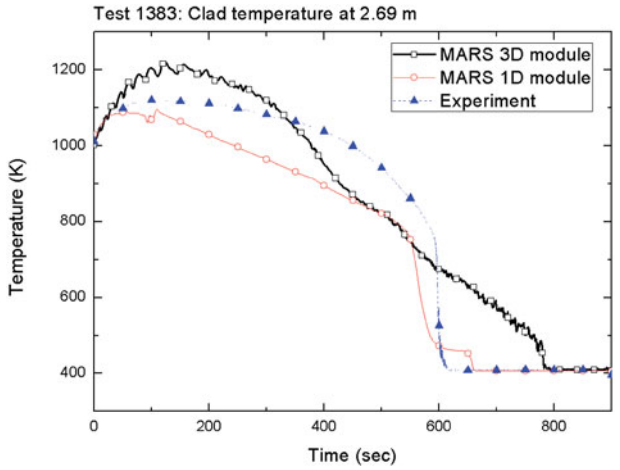

Figure 20. Cladding temperatures with time of Test 1383 at 2.69 m.

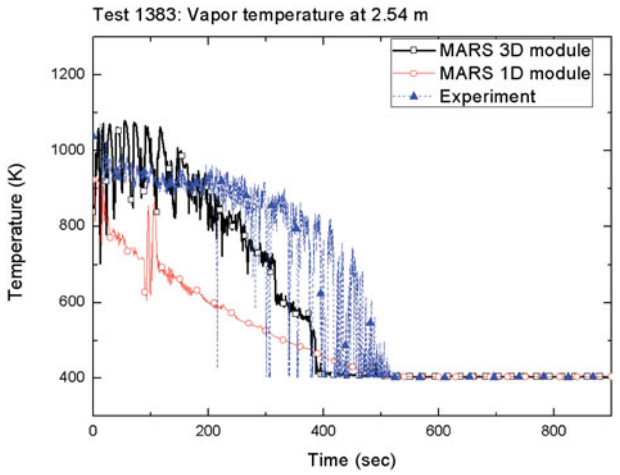

Figure 22. Vapor temperatures with time of Test 1383 at 2.54 m.

especially at the upper region (2.69 m). In the experiment as shown in Figure 20, after reaching the PCT, the cladding temperature decreases very slowly for about 500 sec. Afterward, once the heater rod is quenched, a rapid temperature drop is observed. However, the 1D and 3D modules predict different cooling patterns. After reaching the PCT, the temperature simulated by the 1D module decreases quickly, and is observed as underpredicted in this time period. On the other hand, in the beginning of the reflood, the temperature simulated by the 3D module is overpredicted until about 350 sec. Since then, the cladding temperature calculated decreases gradually, and goes below the experimental data until 600 sec. The entire quench front locations are shown in **Figure 21**. Similar to the case of Test 1285, reasonable quenching times were predicted although slightly fast quenching times were observed in the lower and middle regions.

Figure 22 shows the vapor temperatures predicted and measured for Test 1383 with time at the elevation of

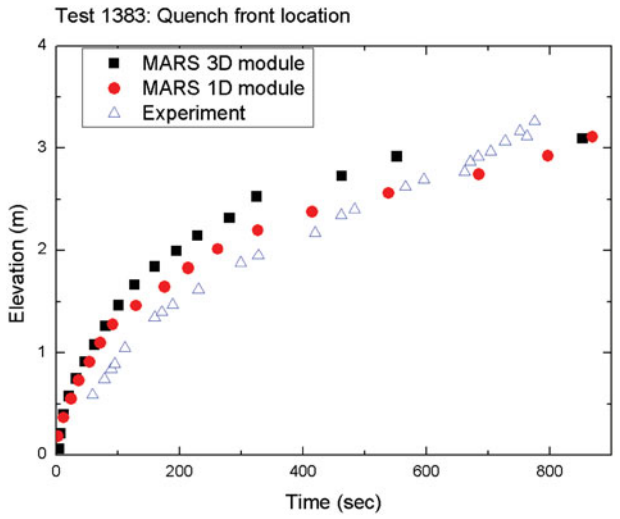

Figure 21. Quench front location of Test 1383.

2.54 m. The vapor temperatures show similar behaviors in the cladding temperatures. In the early phase, the vapor temperature calculated by the 3D module is slightly higher, and the trend is reversed at about 200 sec. Moreover, the vapor temperatures predicted by the 1D module is far below that by the 3D module and experimental results. Thus, the overall prediction using the 3D module shows the improved results as compared to the 1D module. In addition, the underestimated values by the 3D module in the cladding and vapor temperatures indicate that more active interfacial heat transfer is calculated between the liquid and vapor phases as compared with the experimental data. This observation also implies the overpredicted amount of liquid in the rod bundle by the 3D module.

The underpredicted cladding and vapor temperatures are consistent with a recent assessment work on a modification of the COBRA-TF code by Ergun and coworkers [9–11]. To improve the dispersed flow film boiling model in the code, they introduced a new small droplet field with modifying other three fields (vapor, liquid, and large droplet) [9,10]. In the assessment work with the RBHT experimental data, underpredicted cladding and vapor temperatures were observed at the upper region (2.69 and 2.54 m). Their analysis indicated that underpredicted interfacial drag caused more liquid in the rod bundle. This overestimated liquid led to a more active cooling effect, and finally lower vapor and cladding temperatures were predicted. Thus, the modification of the droplet entrainment and interfacial drag models with adding the small droplet field resulted in improved predictions including the quench front behavior. The small droplets are dragged upward by the vapor, and less liquid remains in the bundle as compared with the result by the original code although the earlier quenching behavior is still predicted in both versions of the code.

Figure 23 shows the collapsed liquid level calculated by the MARS code with the experimental data for Test

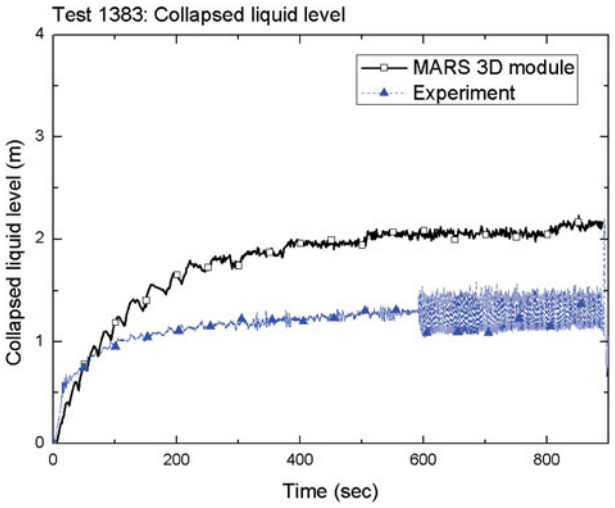

Figure 23. Collapsed liquid level with time of Test 1383.

1383. This liquid level indicates the amount of liquid stored in the bundle. The liquid level computed from the experimental data was determined using bundle differential pressure measurements. The sum of liquid fraction for each volume multiplied by the node length gave the liquid level calculated by the MARS code [22]. Here the 1D module results are omitted since the droplet field is only adopted in the 3D module. As the comparison result presents, the 3D module predicts the overestimated amount of liquid in the upper region, which is a similar tendency to the Ergun et al.'s work discussed above. In addition to the result of Test 1383, **Figure 24** shows the collapsed liquid level of Test 1285. Unlike the case of low flooding rate (Test 1383), the comparison result shows no significant difference between the experimental data and calculation result in the liquid level. Therefore, a modification of the entrainment and interfacial drag models is also needed in the MARS 3D module to predict an accurate quenching behavior. Moreover, the

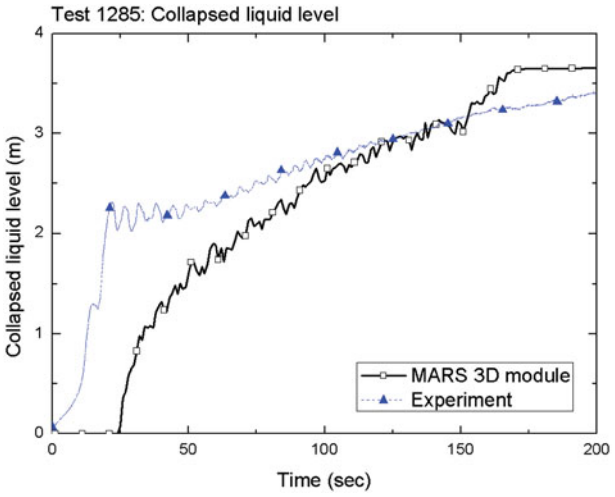

Figure 24. Collapsed liquid level with time of Test 1285.

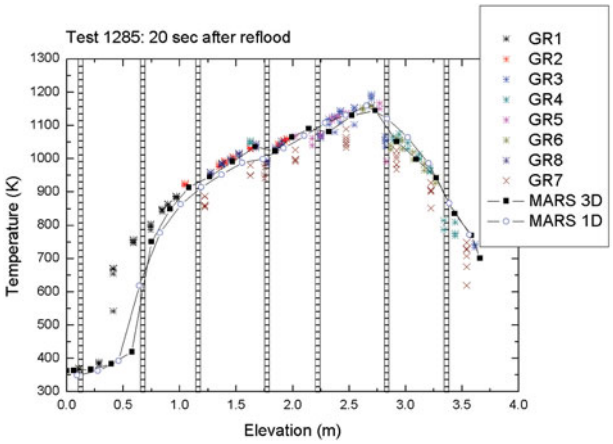

Figure 25. Cladding temperatures with elevation of Test 1285 at 20 sec after reflood.

modifications suggested could give more effective improvement in the case of low flooding rate.

5.3. *Grid effects for the cases of higher and low flooding rates*

The accurate prediction of local peak temperatures is important because the rod bundle part in the test section corresponds to the reactor core. Locations at which peak temperatures occur indicate the place of high failure probability of the structural integrity. Thus, in order to assess the accurate local peak temperature, a local behavior of the temperature near the grids was compared with the experimental data. **Figures 25 and 26** show the comparison of local cladding temperatures at 20 and 40 sec after the injection of the higher flooding rate (Test 1285) begins, and **Figures 27 and 28** show the same kind for the low flooding rate (Test 1385). In addition, the cladding temperature variations magnified near the fourth grid are presented in **Figures 29–32**. As observed, the experimental data show the instantaneous drop near the grids. This is the typical local behavior of

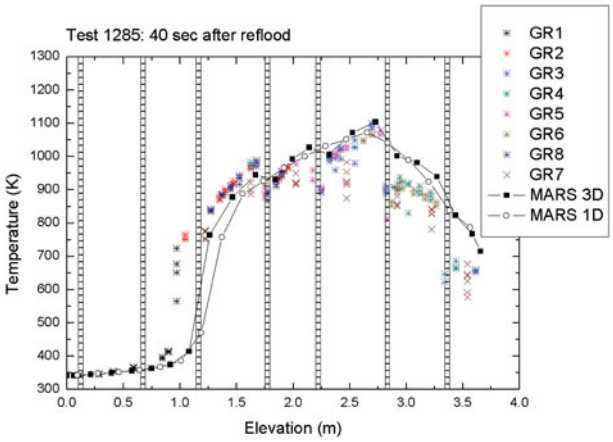

Figure 26. Cladding temperatures with elevation of Test 1285 at 40 sec after reflood.

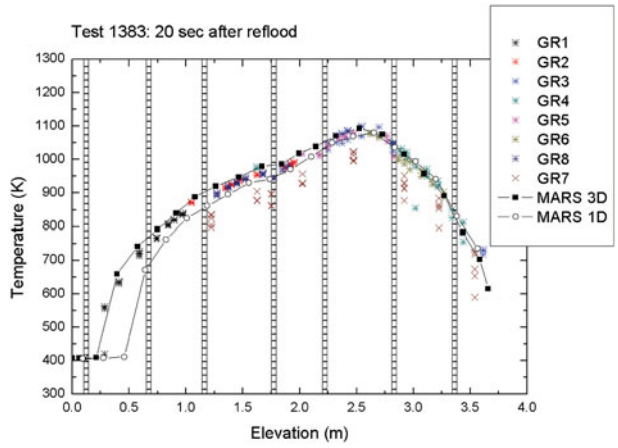

Figure 27. Cladding temperatures with elevation of Test 1383 at 20 sec after reflood.

the cladding temperature due to presence of a grid since a grid takes part in local cooling with mainly three mechanisms, such as grid rewet, convective enhancement, and droplet breakup [3]. Through the simulation results, it is observed that the cladding temperatures calculated by the 1D module gradually increases with elevation without showing the temperature drop near the grids. The temperature profile by the 1D module shows a gradual increase from the lower region to the peak power point and a gradual decrease from that point to the upper region. On the other hand, however, the cladding temperatures predicted by the 3D module drop locally near the third and fourth grids. In addition, the temperature profile simulated by the 3D module shows the accurate elevations of the local peak temperatures compared with those of the experiments. Moreover, this additional cooling effect due to the grids becomes noticeable as time passes. The results of the Test 1285 show this tendency clearly as shown in Figures 29 and 30. As stated above, this cooling pattern near the grids is not reflected properly in the MARS 1D module due to the absence of a relevant grid model in the current code version.

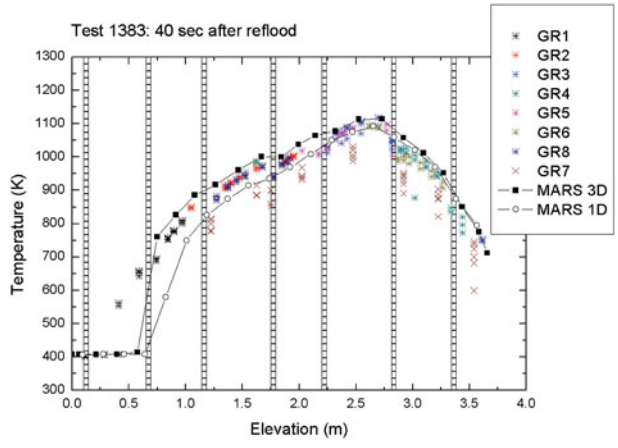

Figure 28. Cladding temperatures with elevation of Test 1383 at 40 sec after reflood.

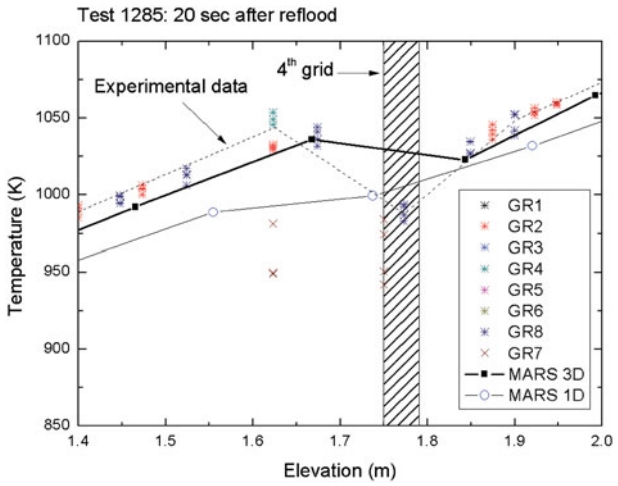

Figure 29. Cladding temperatures near the fourth grid (1.4–2.0 m) of Test 1285 at 20 sec after reflood.

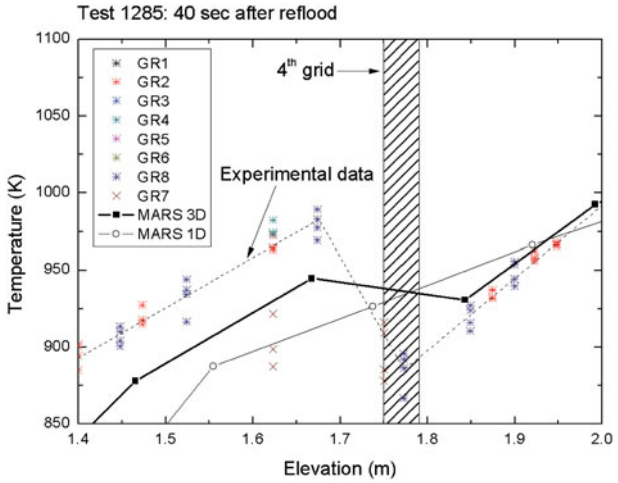

Figure 30. Cladding temperatures near the fourth grid (1.4–2.0 m) of Test 1285 at 40 sec after reflood.

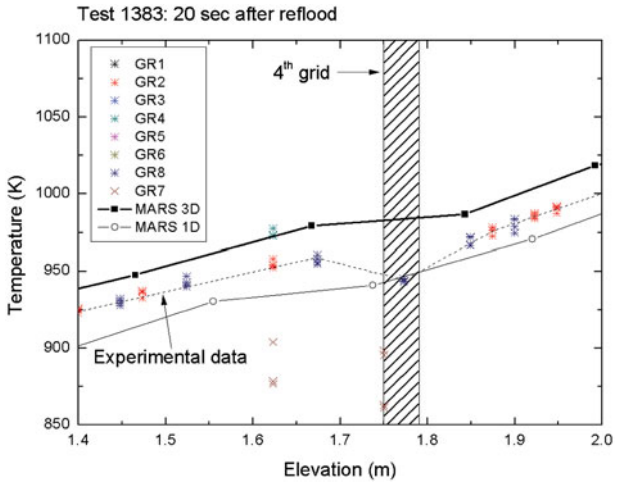

Figure 31. Cladding temperatures near the fourth grid (1.4–2.0 m) of Test 1383 at 20 sec after reflood.

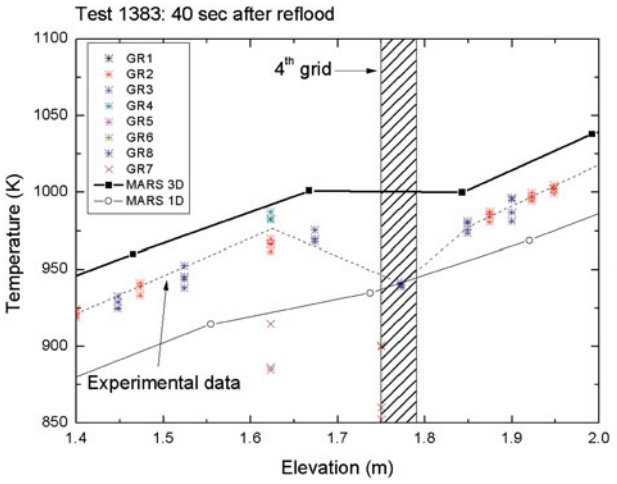

Figure 32. Cladding temperatures near the fourth grid (1.4–2.0 m) of Test 1383 at 40 sec after reflood.

However, by simulating the RBHT experiments using the grid model implemented in the 3D module, the similar local temperature behavior to the RBHT experimental data could be captured accurately although the amount of the temperature decrease calculated is slightly lower. Therefore, the MARS 3D simulation is expected to be accurate in estimating the reflood heat transfer phenomena in terms of overall tendency of cladding temperature and local temperature drop near the grids.

6. Conclusion

In this study, the MARS assessment was carried out using the RBHT experimental data under different flooding rates of 0.0254 and 0.1524 m/sec. As compared to the MARS 1D simulation, significant efforts have been made to the MARS 3D simulation to improve the prediction capability for the reflood heat transfer problem. Representative cases of Tests 1285 and 1383 of the RBHT experiments were compared with the calculation results of the MARS 1D and 3D modules, and major findings are summarized as follows:

(1) The overall prediction of the cladding temperatures and PCTs using the MARS 1D and 3D modules was in a good agreement with the RBHT experimental data with the better simulation results by the 3D module.
(2) The vapor temperatures by the 1D and 3D modules showed a different cooling pattern as compared with the experimental data after reaching the maximum values. The 1D module predicted a gradual and fast decrease for both the test cases while an improved prediction was observed in the results of the 3D module, which suggests that the droplet field plays an important role in simulating the DFFB regime.
(3) In general, the quenching times were reasonably predicted, especially in the lower and middle regions of the test section although the earlier quenching times were observed in the simulations by both the modules. The similar tendency of fast quenching is also reported in other assessment studies with system safety codes.
(4) Moreover, in the lower flooding rate, the amount of liquid stored in the bundle calculated by the 3D module affects significantly the cooling pattern in the vapor and cladding temperatures, rather in the higher flooding rate.
(5) As compared to the simulations by the 1D module, the 3D module predicted the more similar temperature profiles to the experimental data along the elevation. Tendency of local temperature drop near the grids was captured successfully using the MARS 3D module with the help of the implemented grid model. Consideration of the local cooling effect by the grids is important in predicting accurate positions of the local peak temperatures although the amount of temperature drop near the grids is underpredicted.
(6) In the future, local flow parameters such as cross flow and vortex flow need to be analyzed for a more accurate prediction of quenching behavior.

Current MARS code analysis may not give very detailed interpretation about local phenomena. Nonetheless the code may provide meaningful information about interpreting the complex two-phase phenomena. Although there are still many areas that need to improve to understand the experimental results, utilization of MARS and trying to find a weakness is still meaningful for further code development.

Acknowledgements

The authors thank Dr Seung Hoon Ahn of Korea Institute of Nuclear Safety for providing the RBHT raw data and advising MARS simulation.

Funding

This work was supported by the research fund of Hanyang University [grant number HY-2011-N].

Nomenclature

g	Gravity, 9.8 m^2/sec
$\dot{m}$	Mass flow rate (kg/sec)
P	Power or pressure
Re	Reynolds number
S	Entrainment rate (kg/sec)
u	Velocity (m/sec)
We	Weber number

Greek letters

α	Thermal diffusivity (m^2/sec)
Δ	Difference
ρ	Density (g/m^3)
σ	Surface tension (N/m)

Subscriptions

avg	Average
crit	Critical
d	Drag
D	Drag or diameter
E	Entrainment
max	Maximum
min	Minimum
v	Vapor

Abbreviations

DBA	Design basis accident
DFFB	Dispersed flow film boiling
LOCA	Loss of coolant accident
LOFA	Loss of flow accident
PCT	Peak cladding temperature
PWR	Pressurized water reactor
RBHT	Rod Bundle Heat Transfer

References

[1] Lee N, Wong S, Yeh HC, Hochreiter LE. PWR FLECHT-SEASET unblocked bundle, forced and gravity reflood task data evaluation and analysis report. Monroeville (PA): Westinghouse Electric Corporation; 1982. (EPRI NP-2013; NUREG/CR-2256; WCAP-9891).

[2] Ihle P and Rust K. FEBA – flooding experiments with blocked arrays evaluation report. Karlsruhe (Germany): Karlsruhe Institute of Technology, Kernforschungszentrum Karlsruhe; 1984. (KfK 3657).

[3] Division of Systems Research. Compendium of ECCS research for realistic LOCA analysis. Washington (DC): US Nuclear Regulatory Commission; 1988. (NUREG - 1230. R4).

[4] Deruaz R, Clement P, Veteau JM. Study of two-dimensional effects in the core of a light water reactor during the ECC's phase following a loss of coolant accident. Brussels (Luxembourg): Commission of the European Communities (EU); 1985. (EUR 10076 EN).

[5] Hochreiter LE, Cheung F.-B, Lin TF, Baratta AJ, Frepoli C, Sridharan A, Todd DR, Rosal ER. Dispersed flow heat transfer under reflood conditions in a 49 rod bundle: test plan and design – results from tasks 1–10. University Park (PA): US Nuclear Regulatory Commission; 2001. (PSU ME/NE-NRC-04-98-041 Report 1, Revision 1).

[6] Choi TS, No HC. Improvement of the reflood model of RELAP5/MOD3.3 based on the assessments against FLECHT-SEASET tests. Nucl Eng Des. 2010;240:832–841.

[7] Choi TS, No HC. An improved RELAP5/MOD3.3 reflood model considering the effect of spacer grids. Nucl Eng Des. 2012;250:613–625.

[8] Cho HK, Choi KY, Cho S, Song C-H. Experimental observation of the droplet size change across a wet grid spacer in a 6 × 6 rod bundle. Nucl Eng Des. 2011;241:4649–4656.

[9] Ergun S. Modeling of dispersed flow film boiling with two flow, five field Eulerian-Eulerian approach and effects of spacer grids on heat transfer [dissertation]. University Park (PA): The Pennsylvania State University; 2006.

[10] Ergun S, Hochreiter LE, Mahaffy JH. Modifications to COBRA-TF to model dispersed flow film boiling with two flow, four field Eulerian–Eulerian approach – part 1. Ann Nucl Energy. 2008;35:1663–1670.

[11] Ergun S, Hochreiter LE, Mahaffy JH. Modifications to COBRA-TF to model dispersed flow film boiling with two flow, four field Eulerian–Eulerian approach – part 2. Ann Nucl Energy. 2008;35:1671–1676.

[12] Jeong J-J, Bae SW, Hwang DH, Lee WJ, Chung BD. Hot channel analysis capability of the best estimate multi-dimensional system code, MARS 3.0. Nucl Eng Technol. 2005;37:469–478.

[13] Thermal-Hydraulic Safety Research Department. MARS code manual volume I: code structure, system models, and solution methods. Daejeon (Republic of Korea): Korea Atomic Energy Research Institute; 2009. KAERI/TR-2812/2004.

[14] Thermal-Hydraulic Safety Research Department. MARS code manual volume II: input requirements. Daejeon (Republic of Korea): Korea Atomic Energy Research Institute; 2009. KAERI/TR-2811/2004.

[15] Thermal-Hydraulic Safety Research Department. MARS code manual volume IV: developmental assessment report. Daejeon (Republic of Korea): Korea Atomic Energy Research Institute; 2009. KAERI/TR-3042/2005.

[16] Hochreiter LE, Cheung F-B, Lin TF, Frepoli C, Sridharan A, Todd DR, Rosal ER. Rod bundle heat transfer test facility test plan and design. University Park (PA): US Nuclear Regulatory Commission; 2010. (NUREG/CR-6975).

[17] Rosal ER, Lin TF, McClellan IS, Brewer RC. Rod bundle heat transfer test facility description. University Park (PA): US Nuclear Regulatory Commission; 2010. (NUREG/CR-6976).

[18] Hochreiter LE, Cheung F-B, Lin TF, Spring JP, Ergun S, Sridharan A, Ireland A, and Rosal ER. RBHT reflood heat transfer experiments data and analysis. University Park (PA): US Nuclear Regulatory Commission; 2012. (NUREG/CR-6980).

[19] Thermal-Hydraulic Safety Research Center. Development of nuclear thermal hydraulic verification tests and evaluation technology. Daejeon (Republic of Korea): Korea Atomic Energy Research Institute; 2007. KAERI/RR-2706/2006.

[20] Todd DR, Frepoli C, Hochreiter LE. Development of a COBRA-TF model for the Penn State University – Rod Bundle Heat Transfer program. Proceedings of the 7th International Conference on Nuclear Engineering; 1999 Apr 19–23; Tokyo (Japan).

[21] Ha K-S, Jeong J-J, Sim SK. Improvement of liquid droplet entrainment model in the COBRA-TF Code. Nucl Eng Technol. 1998;30:181–193.

[22] Thurgood MJ, Guidotti TE, Sly GA, Kelly JM, Kohrt RJ, Crowell KR, Wikins CA, Cuta JM, Bian SH. COBRA/TRAC-A thermal-hydraulics code for transient analysis of nuclear reactor vessels and primary coolant systems, Vol. 4: developmental assessment and data comparisons. Washington (DC): US Nuclear Regulatory Commission; 1983. (NUREG/CR-3046).